

## **CHARACTERISTICS OF THE T-220HT HALL-EFFECT THRUSTER\***

John B. McVey and Edward J. "Ned" Britt  
Pratt & Whitney Space Propulsion, San Jose, CA

Scott F. Engleman and Frank S. Gulczinski  
Air Force Research Laboratory, Edwards AFB, CA

Edward J. Beiting and James E. Pollard  
The Aerospace Corporation, El Segundo, CA

### **ABSTRACT**

In recent tests the plume current density profile, plume ion energy, and radiated EMI were characterized for Pratt & Whitney's T-220HT Hall Effect thruster. The T-220HT is a high power (6-20 kW) thruster designed for maximum peak thrust. Tests covered a power range from 8-10 kW and discharge voltages of 300 and 600 V. Plume measurements at Air Force Research Laboratory (AFRL) facilities demonstrated plume widths narrower than typical Hall thrusters. Half-angles containing 90% of the integrated plume flux were in the range of 27-29°. Radiated electromagnetic emissions were measured over a frequency range from 200 MHz to 60 GHz at The Aerospace Corporation. For discharge voltages at or below 300 V, EMI was below MIL-STD 461E limits except at a single peak below 1.4 GHz, where the limit was exceeded by only about 5 dB. Increasing the discharge voltage to 600 V noticeably increased emissions in this frequency range, but these were still generally below MIL-STD 461E. Plume ion energy spectra were also characterized at The Aerospace Corporation's facility. An RPA (Retarding Potential Analyzer) was mounted at a downstream distance of 1 meter and was varied in position from 20° to 100° from the thruster centerline. Measurements generally confirmed the plume profile data taken at AFRL. Energy spectra confirm that the flux at high angles is dominated by low energy charge-exchange ions.

### **INTRODUCTION**

The Pratt & Whitney T-220HT, shown in Figure 1, is a high-power Hall Effect Thruster designed for applications in the power range of 6-20 kW. Previous

testing at University of Michigan facilities has extensively mapped thrust and specific impulse over the power range 2-22 kW, with maximum thrust exceeding 1 Newton.<sup>1</sup> In addition to performance characterization, spacecraft interaction issues must be well characterized. The present work is therefore concerned with investigating the plume profile, plume energy, and radiated electromagnetic emissions (EMI) over a power range in the middle of the thruster's operating region. Plume profile measurements were performed at facilities of the Air Force Research Laboratory Propulsion Directorate's Spacecraft Propulsion Branch and confirmed by tests at facilities of The Aerospace Corporation. EMI characterization and plume energy measurements were performed at Aerospace Corporation facilities.

### **T-220HT Thruster**

The T-220HT design is similar to that of the T-220 Hall thruster tested by NASA for 1000 hours<sup>2</sup>, but has been optimized for peak thrust at a given power level. A nominal operating power of  $9 \pm 2$  kW has been identified as the baseline. The thruster has a channel outer diameter of 220 mm and a channel width of 32 mm. An EPL 625-series hollow cathode, with a current emission capability of 100 Amperes, is used as an electron source. The magnetic circuit consists of independent inner and outer electromagnet coils and flux guides.

---

\* Copyright © 2003 E.J. Britt, Pratt & Whitney, San Jose. Published by the American Institute of Aeronautics and Astronautics, Inc., with permission.



**Figure 1. T-220HT mounted in vacuum chamber #3 at AFRL.**

### PLUME PROFILE CHARACTERIZATION

#### AFRL Test Facility

All testing was conducted in AFRL's vacuum chamber #3. Vacuum chamber #3 is a horizontal cylinder 3 meters in diameter and 10 meters long. It has a 2 stage pumping system consisting of mechanical and cryogenic pumping. The mechanical system uses a dry rough pump followed by a turbomolecular pump, which continues to operate during testing to remove light gasses such as helium and hydrogen. Cryogenic pumping is accomplished with four 6 foot panels and four 8 foot panels, which each contain flow lines of Polycold<sup>®</sup> and super-cooled gaseous helium. The panels operate at 20 to 30 K and provide the chamber with approximately 150,000 liters per second of xenon pumping and a base pressure of  $10^{-7}$  torr. The chamber is lined with ½ inch thick, 99%-pure carbon plates to cover all exposed metal surfaces. This carbon plate minimizes the back-sputter of metals onto the thruster. Acquisition of chamber and thruster telemetry is accomplished using a workstation running LabView<sup>®</sup> 6.1 to interface with the attached instrumentation. A data-sampling rate of 1 Hz is nominal for up to 80 separate parameters.

The propellant feed assembly consisted of four manual valves, a 250-sccm flow controller for the cathode, and a 1000-sccm flow controller for the anode. Separate power supplies were used to run the anode discharge, cathode, heater, and the inner and outer magnets.

The T-220-HT was positioned on the test stand facing the cryopanel and pointed axially down the center of the chamber (see Figures 1 and 2). The thruster was aligned relative to the center of the hemispherical array of Faraday probes. This alignment is done with the use

of a dual laser alignment system that references fixed locations within the chamber (see Figures 3 and 4).

The Faraday probes are designed to measure the current density of the HET plume. These probes are arranged every  $15^\circ$  around a semicircular aluminum pipe at a distance of 96 cm. from the center of the T-220HT exit plane. The position of the probes on the probe mount allows them to constantly face the exit plane of the thruster as it moves through a hemispherical route through the plume of the HET. Vertical spacing of the probes along the probe mount is defined as  $\phi$ , while the horizontal sweep angle through the plume is defined as  $\theta$  (see Figure 5).  $\phi$  is defined such that  $90^\circ$  is straight up,  $0^\circ$  is along the chamber centerline, and  $-90^\circ$  is straight down. Ten Faraday probes were positioned on the rake, every  $15^\circ$  from  $\phi = 75^\circ$  to  $\phi = -60^\circ$ . An additional probe was located at  $\phi = 0^\circ$ , facing away from the thruster to measure background or reflected ions. Another probe was located at a fixed position on chamber centerline, 4.18 m downstream of the thruster exit. Resolution in the  $\phi$  position is limited to fixed points on the rake of  $15^\circ$ .  $\theta$  is defined such that when facing downstream,  $\theta = -90^\circ$  is to the right,  $\theta = 0^\circ$  is on chamber centerline, and  $\theta = +90^\circ$  is to the left. The motion of the rake limits the resolution in  $\theta$  to  $0.1^\circ$ .

Ion current density is experimentally determined by using an ion collector that consists of a negatively biased disk of molybdenum and a concentric molybdenum guard ring. The collector is biased negatively to repel electrons. The guard ring is biased to the same value as the collector, such that a uniform sheath exists across the collector. Precision current shunts are located externally and the voltage drop across these shunts is measured in order to determine the current. Current shunts are sized so that biases on the collector and guard ring remain equal to each other. The ion collectors are approximately  $1^\circ$  wide at 96 cm. A step size of  $0.5^\circ$  in  $\theta$  was used to provide high fidelity data.

The Faraday probe bias voltage is selected based on the ion saturation point of the probes; in this case, experimentally determined to be less than  $-20$  V. The first step of the data acquisition program is scanning and recording the voltage drop across all the shunts three times. Next the bias voltage is measured and recorded. Because the bias voltage is fixed, it is

- AFRL Test Facility - 150,000 L/s (Xenon), 3 m diam. × 10m long

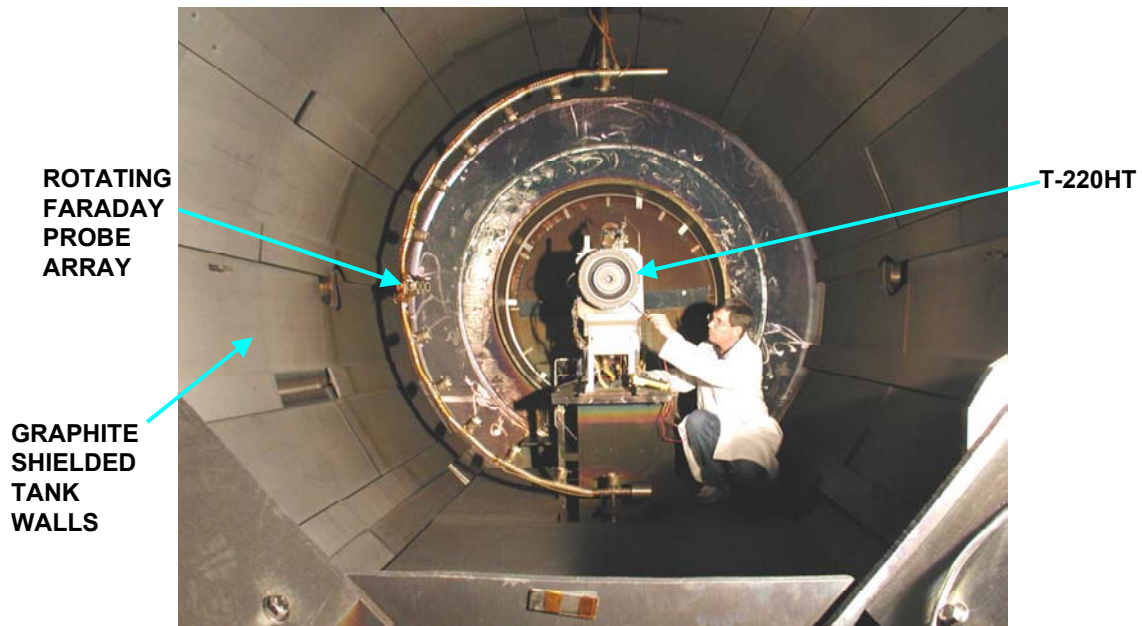


Figure 2. P&W test engineer conducting a final checkout of the T-220-HT inside chamber #3.



Figure 3. Laser alignment verification. The beam can be seen skimming the face of the thruster, then hitting the center of the  $\phi = 0^\circ$  probe at the  $\theta = +90^\circ$  position.

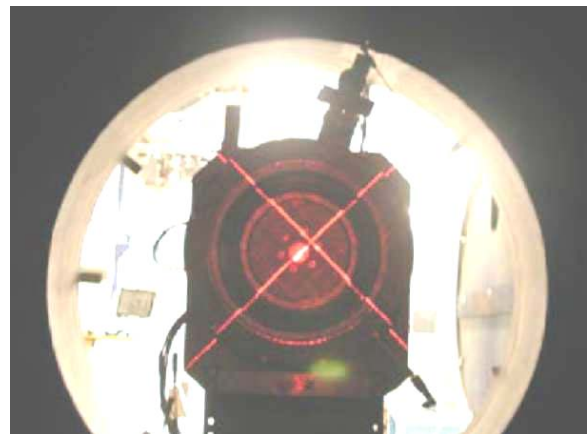
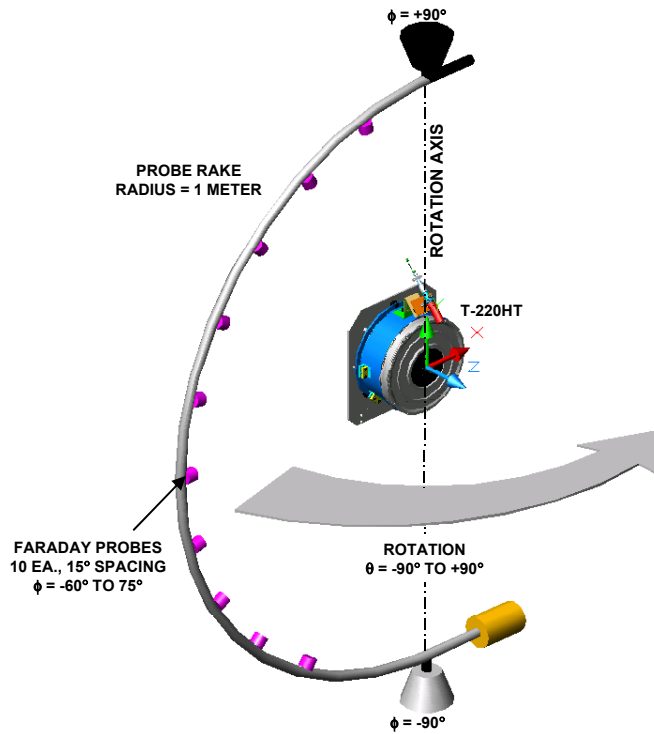


Figure 4. With the rake at the  $\theta = 0^\circ$  position, an alignment laser is used to check that the probe face is level and perpendicular to the thruster face.



**Figure 5. Illustration of AFRL Faraday probe rake and coordinate systems. Rake is shown positioned at  $\theta = -90^\circ$ .**

scanned only once. The program then commands the rake to move  $0.5^\circ$  and records the position. This process is repeated for a complete  $180^\circ$  sweep through the HET plume. Once completed, the voltage drops are converted to currents and then checked to see that the measured values are within 1% of each other for each probe, at each location. A thermocouple was attached to the probe at  $\phi = 0^\circ$  to verify that the rake temperature stays below  $200^\circ\text{C}$ , the melting point of the Kapton<sup>®</sup> tape used for electrical insulation.

#### Test Description

A summary of the power levels and discharge voltages at which plume measurements were taken is shown in Table 1. Inner and outer magnet currents were adjusted so as to minimize both the discharge current for a fixed anode flow rate and the discharge current oscillations. Focussing of the plume is affected by the ratio of currents in the inner and outer magnet coils. Table 2 lists the values for these currents and their ratios for the test conditions used. Tank pressure, measured using an ion gauge calibrated for xenon, varied from  $1.8 \times 10^{-5}$  torr at the lowest flow rates (the 9 kW, 600 V condition) to  $3.4 \times 10^{-5}$  torr at the highest flow rate (the 10 kW, 300 V condition).

A total of 10 Faraday sweeps were made through the plume. Two or three sweeps were made through the plume at each setting, with a third sweep made only if a discrepancy was found between the first two.

**Table 1. Matrix of test conditions.**

Power (kW)	Voltage (V)
8	300
9	300
10	300
9	600

**Table 2. Inner and outer magnet currents.**

Test Conditions	Inner Magnet Current (A)	Outer Magnet Current (A)	Inner / Outer Current
8 kW, 300 V	24.6	20.1	1.2
9 kW, 300 V	25.1	21.2	1.2
10 kW, 300 V	25.9	24.1	1.1
9 kW, 600 V	25.6	22.7	1.1



**Figure 6. View from behind T-220HT showing probe rake sweeping through the plume.**

### Results

Measured ion current densities are shown as a function of azimuth angle  $\theta$  in Figure 7. Solid lines indicate readings from the Faraday probe at  $\phi = 0^\circ$ , with  $\theta$  the 10 Faraday probes, spaced apart in  $\phi$ , with the probe rake positioned at  $\theta = 0^\circ$ . The correspondence between these indicates good symmetry of the plume at right angles. The current density is slightly higher at the top of the thruster than at the bottom. This might be expected, as the hollow cathode is at the top, and the additional neutral xenon from the cathode would produce a slight surplus of propellant at the top of the thruster.

The expected features are seen in Figure 7. The center of the distribution has a double-peak due to the ring-shaped plasma source. At angles from about  $7^\circ$  to  $30^\circ$  off centerline the distribution falls off exponentially (appearing linear on semi-log plots). At high angles the distribution shows “wings” indicative of charge-exchange plasma resulting from the test tank background pressure.

Symmetry of the plume for negative and positive  $\theta$  is very good for most of the distribution, but the peak currents are slightly higher for negative angles than for positive angles, with the difference being about  $2 \text{ mA/cm}^2$ . Initially this effect was attributed to outgassing from the Faraday probe when it first entered the dense part of the plume, as tank pressure was seen to increase noticeably at this point. However, the effect was later confirmed by the plume measurements done at Aerospace Corporation, where the same asymmetry was obtained when sweeping the probe in either direction. The cause is not yet completely understood. The cathode is slightly farther from the discharge at negative  $\theta$ , since it is positioned at  $5^\circ$

clockwise from top dead center, which might be expected to produce a current asymmetry opposite to the one seen. Future tests will attempt to reproduce this effect and then change the polarities of the inner and outer magnets. If the maximum current density reverses position, then a magnetic effect is indicated; if not, then an asymmetry in the xenon flow from the anode may be responsible.

Figure 8 compares the measured plume distribution shapes with the current densities normalized at  $-20^\circ$ . The close agreement in the exponentially-falling region illustrates that all the distributions decrease at very similar rates, independent of power or discharge voltage.

### Plume Profile Analyses

The parameter used here to evaluate and compare plume widths from various Hall Effect thrusters is the half-angle containing 90% of the integrated flux. This angle can be evaluated analytically. The fraction  $F$  of integrated flux contained by a half-angle  $\theta$  is given by:

$$F(\theta) = \frac{\int_0^\theta j(\theta') \sin(\theta') d\theta'}{\int_0^{\pi/2} j(\theta') \sin(\theta') d\theta'} \quad (1)$$

Evaluation consists of performing the integrals for a given plume distribution  $j(\theta')$  and finding the value of  $\theta$  that makes  $F(\theta) = 0.9$ .

Calculation of the plume width half-angle must take into account the charge-exchange plasma “wings” at high angles (see Figure 8). These are an artifact of the test tank environment and should not be included in evaluation of the integrated flux. The charge-exchange “wings” were analytically removed from the measured plume profiles by extrapolation of their exponentially decreasing portions. Eq. (1) was then used to calculate 90% half-angles for the negative and positive angle portions of the profiles, respectively. The results are given in Table 3.

**Table 3. Half-angles containing 90% of the integrated flux.**

Test Condition	90% Half Angle (deg)		
	angle < 0	angle > 0	average
8 kW, 300 V	27.2	28.8	28.0
9 kW, 300 V	27.1	29.7	28.4
10 kW, 300 V	26.0	28.2	27.1
9 kW, 600 V	29.2	28.6	28.9

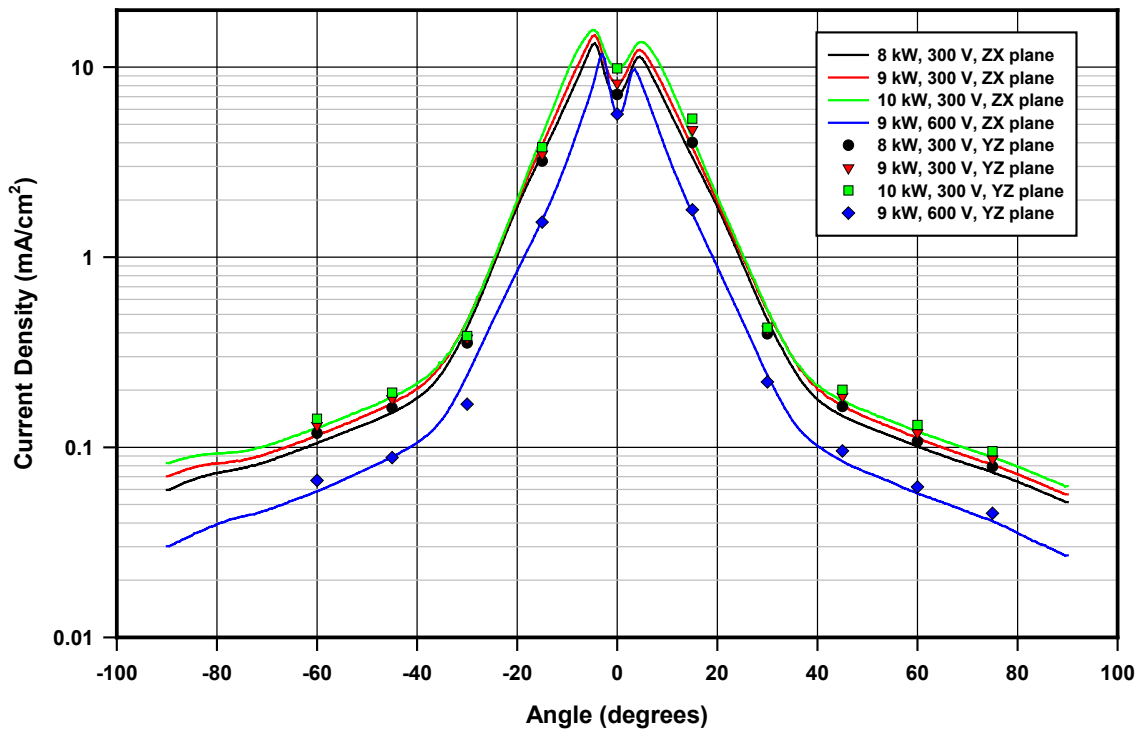


Figure 7. Measured ion current density profiles.

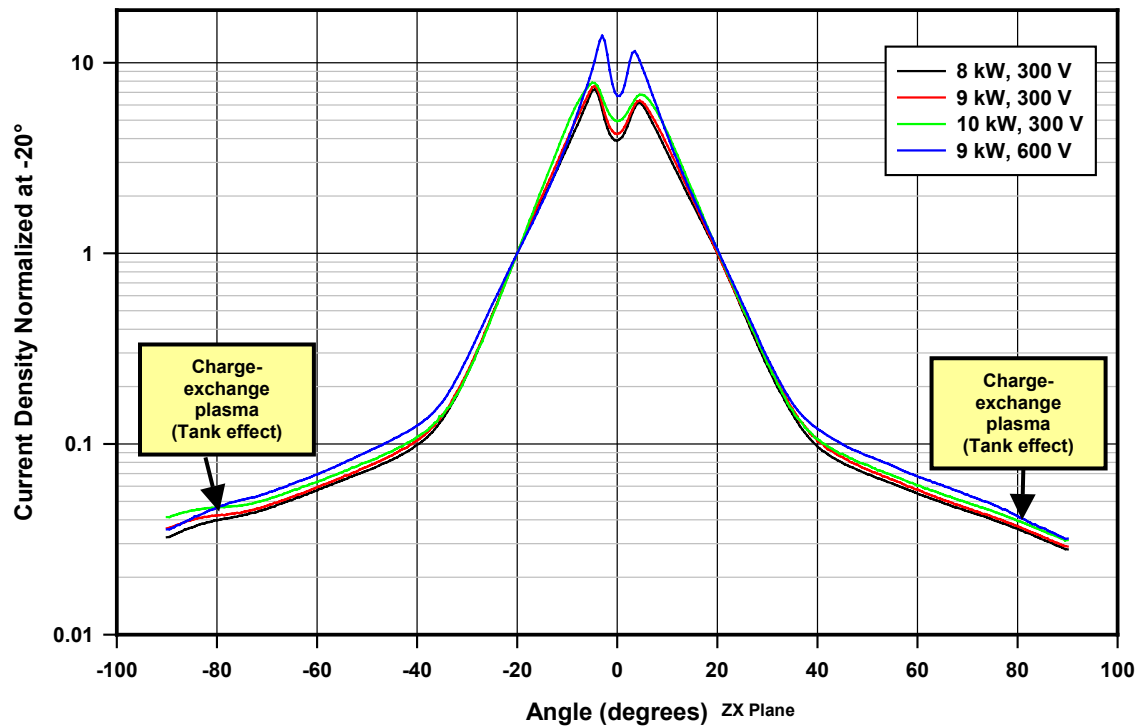


Figure 8. Comparison of plume profiles with current densities normalized at -20°.

## Plume Profile Comparison

The identical plume width evaluation procedure outlined above, including removal of the charge exchange wings, has been performed on various Hall thrusters for which plume profile data exist in the open literature or have been developed by Pratt & Whitney. The resulting cone half-angles are shown in Table 4. As shown, the T-220HT plume is the narrowest of the thrusters evaluated.

**Table 4. Comparison of plume width data for various Hall thrusters.**

Manufacturer & HET	Half-Angle, 90% Flux	Source of Data
P&W T-220HT	28-29°	Present work
P&W T-140	32°/29°	Measurements at U. of Michigan <sup>3</sup>
Primex BPT 4000A	33°	AIAA 99-2573, 1999 JPC <sup>4</sup>
FAKEL SPT-140	43°	AIAA 00-3521, 2000 JPC <sup>5</sup>
FAKEL SPT-100	>45°	Measurements at NASA GRC <sup>6</sup>

## EMI CHARACTERIZATION

### Aerospace Corp. Test Facility

The Aerospace Corporation EMC facility, in which the T-220HT EMI measurements were performed, has been discussed in detail in previous publications.<sup>7</sup> A schematic of the facility is shown in Figure 9. The thruster was mounted in the all-dielectric vacuum tank that mates to a stainless steel vacuum chamber with a nominal pumping speed of 220,000 liter/sec for xenon. A semi-anechoic room surrounds the dielectric tank to shield the thruster from the ambient electromagnetic environment. A set of calibrated receivers recorded the radiation emanating from the thruster over the frequency range from 0.2 to 60 GHz. Below 18 GHz, the receiver connects sequentially to a series of antennas through a panel in the semi-anechoic room using a two-section semi-rigid cable with known attenuation. Above 18 GHz, a smaller receiver situated in the anechoic room connects sequentially through one of two short cables to a series of octave horns.

A photograph of the T220HT in the dielectric tank is presented in Figure 10. The thruster was attached to a Pratt & Whitney-supplied vertical aluminum bracket that was mounted on an aluminum base plate. The base plate was resting on a water-cooled shelf positioned so the centerline of the thruster coincided with the centerline of the fiberglass tank. Propellant

lines were routed along the bottom of the dielectric chamber underneath a fiberglass plate to a vacuum feedthrough in the main chamber. The distance from the fiberglass back flange to the back of the vertical mounting plate was 256 mm.

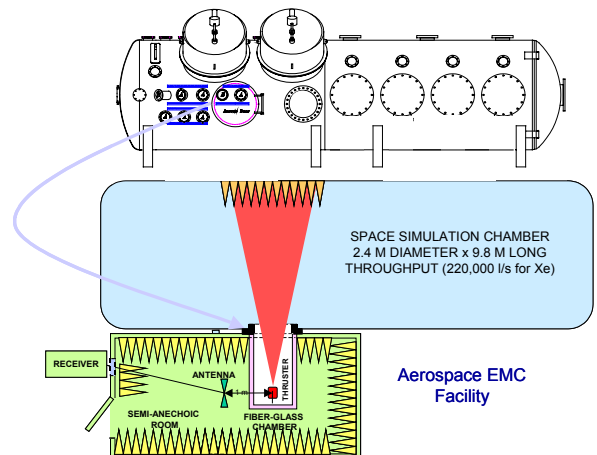


**Figure 9. Layout of the facility used to measure electromagnetic emissions from the T-220HT thruster.**

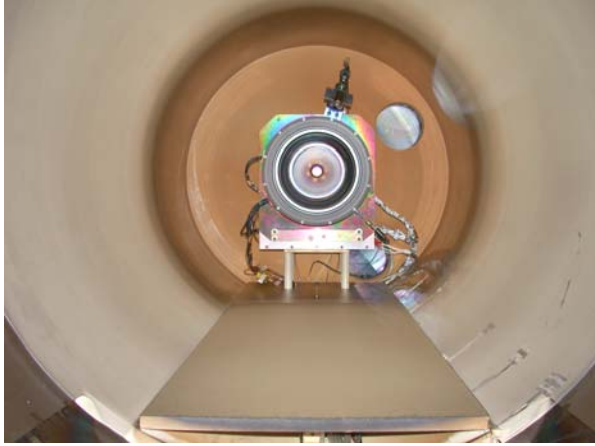


**Figure 10. T220HT thruster mounted in fiberglass tank on a water cooled aluminum plate.**

The thruster was operated with laboratory power supplies provided by Pratt & Whitney. Cathode flow was set by a calibrated mass flow controller and anode flow was set using a metering valve to achieve the desired discharge current. Pressures measured in the main chamber during the EMI tests for the four operating conditions of the T220HT are given in Table 5. The pressures behind the thruster in the fiberglass tank are approximately three times those measured in the main chamber.

**Table 5. Main Chamber Pressure for T220HT Operating Conditions During EMI Tests.**

Thruster Voltage (V)	Thruster Current (A)	Thruster Power (kW)	Cathode Flow (mg/s)	Corrected Pressure (Torr)
300	20.0	6.0	2.15	$2.0 \times 10^{-5}$
250	36.0	9.0	2.70	$3.1 \times 10^{-5}$
300	30.0	9.0	3.06	$2.8 \times 10^{-5}$
600	15.0	9.0	1.82	$1.7 \times 10^{-5}$

Radiated Electric Field

Electromagnetic radiation was sensed by antennas that meet MIL-STD 461E requirements with the exception that a large double ridge horn was replaced by a log periodic antenna. Signals were routed via cables through a panel in the anechoic room to a Hewlett Packard Model 8572A microwave receiver. Antenna placement next to the fiberglass tank is shown in Figure 11. Care was exercised to shield all cables inside the vacuum chamber leading to the T220HT to mitigate radiation from these conductors.

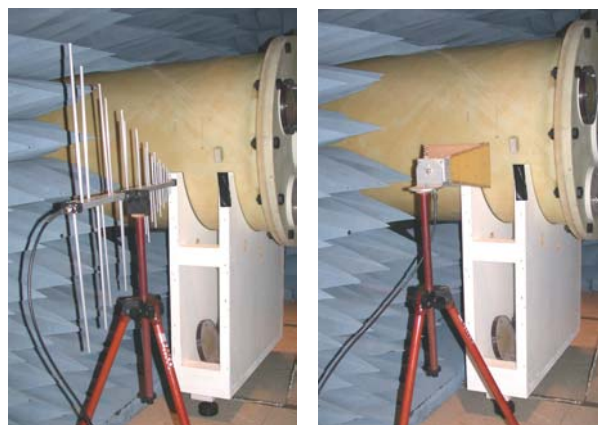


**Figure 11. Positions of the antennas used for the MIL-STD 461E RE102 measurement from 200 MHz to 18 GHz. The log-periodic (left) and double ridge horn (right) are shown in their vertically polarized orientations.**

The bands, resolution bandwidths (RBW), low noise (pre)amplifiers (LNAs), and antennas used for the radiated emission measurements are listed in Table 6. The wavelengths and maximum dimensions of the antennas listed in Table 6 are used to calculate the far field distance shown in the last column in this table. Antennas were placed 1 meter to the side of the thruster as shown in Figure 11. Below 1 GHz, the antennas are in the near field and above this frequency they are in far field, although this demarcation is not exact. Both vertically and horizontally polarized

emission data were acquired for all antennas. The height of the log periodic and double ridge horn antennas was 120 cm above the grounded floor of the semi-anechoic room.

Figures 12-13 are the radiated electric field measurements (MIL-STD 462E RE102) below 18 GHz. In these spectra, the ordinate is dB field strength above  $1 \mu\text{V/m}$ , that is,  $20 \times \log_{10}[(\text{V/m})/1 \mu\text{V/m}]$ . Accordingly, an increase of 20 dB is equivalent to a  $10 \times$  increase in the field. The abscissa is  $\log_{10}(\text{Hz})$ . The instrument noise and anechoic room background are shown on each figure. The instrument noise was recorded with a 50-ohm terminator on the input of the receiver. The semi-anechoic room backgrounds were recorded just before or just after the acquisition on the emission data for each antenna's frequency segment. The discontinuity apparent in the survey and background spectra occurs when the bandwidth is increased by a factor of 10 at 1 GHz (see Table 6).

Observations from these spectra include:

- There is little difference between horizontally and vertically polarized emission at a power of 6 kW; at 9 kW, the horizontally polarized emission was somewhat greater than the vertically polarized emission especially at frequencies greater than 1GHz.
- For a 300 V discharge voltage, emission is greater when the thruster operated at 6.0 kW than when operated at 9 kW below 1GHz and greater for the 9 kW power above 1 GHz.
- At a power of 9 kW, the emission increases markedly with increasing discharge voltage, however, the emission at a discharge voltage of 300 V could be considerably greater than the 600 V near frequencies of 1.4 and 4 GHz.
- Emission exceeds the MIL-STD 461E limits only marginally at selected frequencies below 1.4 GHz.

The spectra from the 18–60 GHz frequency interval are displayed in Figure 14. As expected, there is little emission from the thruster at these frequencies. There is no vertically polarized emission from the thruster above the background level. There is some horizontally polarized emission between 18 and 24 GHz at the 9.0 kW, 250 V operating point. The peak amplitude of these emissions are at least 15 dB below the projected MIL-STD 462E RE102 limit lines.

**Table 6. Electromagnetic Band Parameters**

Bands	Wavelength Ranges	RBW (kHz)*	LNA	Antenna	L (m)	Far Field Distance**
0.2 - 1 GHz	1.5m – 30 cm	100		Log Periodic	0.85	4.5 – 4.8m
1 - 2 GHz	30 – 15 cm	1000		DR Horn	0.2	90 – 54 cm
2 - 18 GHz	15 - 1.67 cm	1000	--	DR Horn	0.2	0.54 – 4.8 m
18 – 26.5 GHz	1.67 – 1.13 cm	1000	Miteq 2	Octave Horn 1	0.054	35 – 52 cm
26.5 – 40 GHz	1.13 – 0.75 cm	1000	Miteq 3	Octave Horn 2	0.034	21 – 31 cm
40 – 50 GHz	0.75 – 0.60 cm	1000	Miteq 4	Octave Horn 3	0.024	15 – 19 cm
50 - 60 GHz	0.60 – 50 cm	1000	Miteq 4	Octave Horn 3	0.024	19 – 23 cm

\*200 MHz – 18 GHz RBW are 6 dB widths whereas 18 – 60 GHz widths are 3 dB widths (taken using Agilent 8565EC analyzer); 3 dB widths are broader than the 6 dB widths of the same numerical value bandwidth by a factor of 1.47.

\*\*Greater of  $3\lambda$  or  $2L^2/\lambda$  where L is the largest antenna dimension.<sup>8</sup>

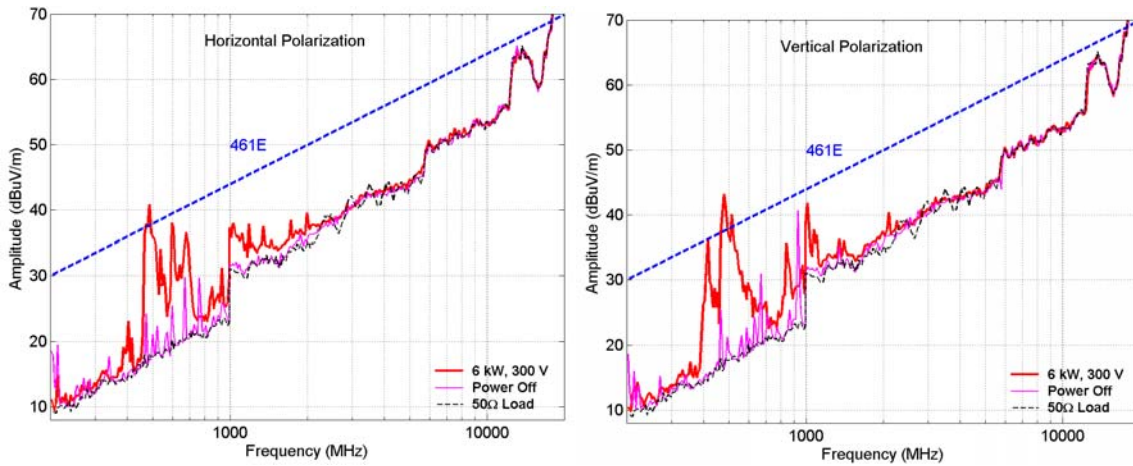


**Figure 12. Horizontally and vertically polarized emission from T220HT operating at 6.0 kW and 300V.**

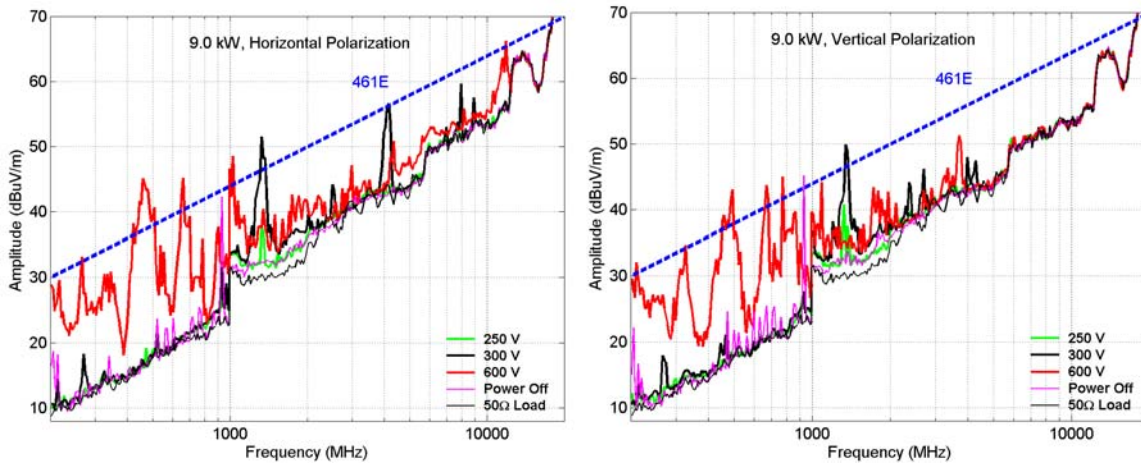


**Figure 13. Horizontally and vertically polarized emission from T220HT operating at 9.0 kW.**

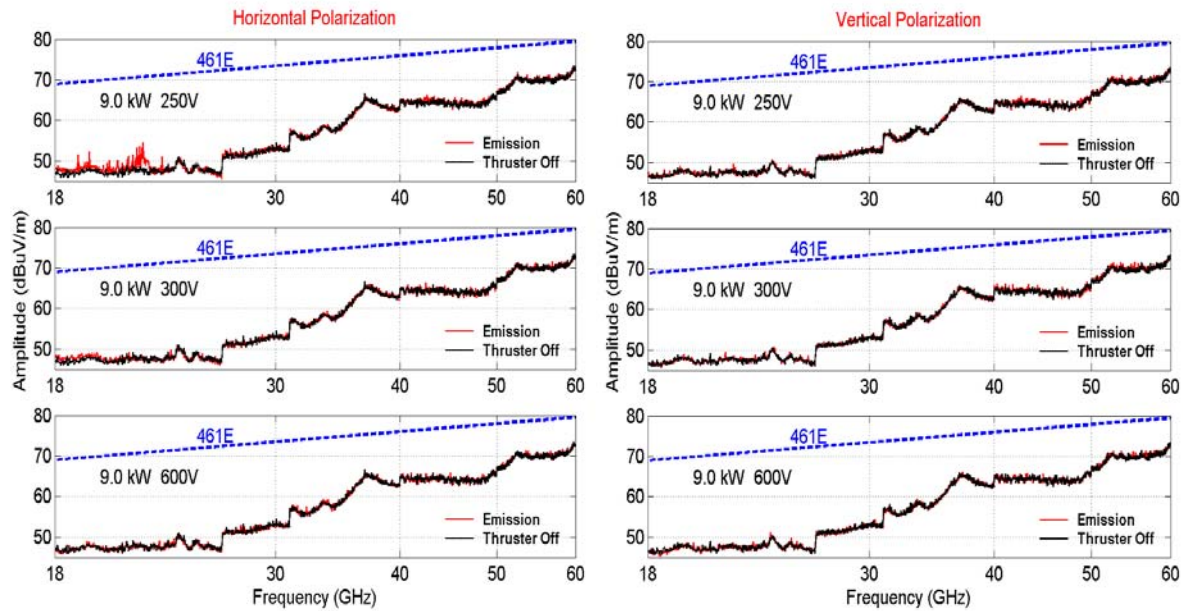


Figure 14. High frequency (18 – 60 GHz) horizontally and vertically polarized survey emission spectra from T220HT at 9.0 kW and three discharge voltages.

## ION ENERGY CHARACTERIZATION

### Test Facility

Measurements of ion flux and energy spectra in the T-220HT plume were performed at The Aerospace Corporation with a setup similar to that used in other recent tests.<sup>9</sup> Background pressure was measured by ionization gauges located on the tank wall adjacent to the thruster (IG1) and in the beam dump region (IG2). With the thruster at 300 V, 30 A the xenon pressures were  $IG1 = 2.0 \times 10^{-5}$  torr and  $IG2 = 2.5 \times 10^{-5}$  torr, using the correction factor of 0.348 specified by the manufacturer for xenon relative to nitrogen.

In order to measure ion flux and energy spectra as a function of position, a retarding potential analyzer (RPA) was mounted in front of the thruster on an arm connected to a turntable, as shown in Figure 15. Distance from the face of the thruster to the RPA was 100 cm. The RPA outer grid was at -20 V relative to ground to exclude electrons. The retarding potential was applied to an inner grid placed between the outer grid and the collector, and the collector was biased at -20 V relative to the inner grid to suppress the collection of electrons (e.g., inner = +300 V, collector = +280 V).

Flux scans were recorded in 2.5° angular steps with the retarding potential ranging from 0 V to 50 V in 25-V steps. Energy scans were recorded in 5° angular steps with the retarding potential ranging from -3 V to +357

V in 6-V steps, or from -6 V to +714 V in 12-V steps. Hence the energy scan extended to voltages greater than  $E/q$  for primary ions, where  $E/q$  is the ion kinetic energy per unit charge. Dividing the slope of the RPA current vs. voltage curve by the collector area ( $3.88 \text{ cm}^2$ ) and by the overall grid transmission (11%) gave the differential flux vs.  $E/q$  in absolute units. A transmission of 11% was based on comparing RPA and flux probe data measured in previous experiments. The RPA was expected to have an absolute accuracy for ion flux of  $\pm 20\%$  with a field-of-view half-angle of approximately 45°.

### Results

#### Plume Profiles

Measured plume profiles are compared in Figure 16 with the data previously obtained at AFRL (see Figures 7 and 8). Current measurements are normalized by the value obtained at -20°, in order to compensate for differences in view factors between the different types of probes and the thruster. Profile shapes measured at the two facilities, using different instrumentation, agree very closely. The fact that the RPA and AFRL's Faraday probes used different bias voltages (see Figure 16) affects the collection of low energy ions, which becomes important for the charge-exchange dominated plume wings; as a result, the RPA measurements are slightly lower in these regions.

### Energy Spectra

Graphs of differential flux vs.  $E/q$  were obtained for angles varying from  $25^\circ$  to  $100^\circ$  in steps of  $5^\circ$ , and are presented in Figures 17 through 20. Thruster operating conditions were the same as those for the plume measurements at AFRL. For angles less than  $25^\circ$  no meaningful data could be obtained because the beam current was large enough to saturate the RPA. Noise seen in some of the data, (the  $45\text{-}75^\circ$  data shown in Figure 20, for example ) is due to operating characteristics of the thruster, not to the RPA.

The spectra confirm that for angles greater than about  $40^\circ$ , the beam current is dominated by low energy ( $< 30$  eV) charge exchange ions. It is expected that this flux of low energy ions would be greatly reduced in the low background pressure of a space environment.

### SUMMARY AND CONCLUSIONS

#### Plume Characterization

A narrow plume width ( $< 30^\circ$ ) was confirmed at the anticipated operating conditions. The plume width is not highly dependent on discharge voltage. Plume profile data taken in two perpendicular planes match reasonably well, indicating good overall plume symmetry. There was a slight asymmetry seen between the peak plume current values at positive and negative angle, which was seen both at AFRL and at The Aerospace Corp.

Plume profile data obtained at Aerospace Corporation confirmed the data taken earlier at AFRL. There were slight differences that were expected as a result of a lower tank background pressure at Aerospace; the fact that these were observed provide confidence that plume intensity at high angles will be very low in a space environment.

Plume energy measurements confirmed that the primary contributor to plume intensity at high angles is low-energy charge exchange plasma, which should be nearly negligible in a space environment.

#### EMI Characterization

Radiated EMI at the operating point of 9 kW/300 V is below MIL-461E everywhere except for a narrow peak at  $\sim 1.3$  GHz, where it is only about 5 dB higher. Measured EMI is barely higher than background for frequencies above 18 GHz. EMI increases with increasing discharge voltage, but is still relatively low at the highest voltage for which measurements were made (600 V).

### ACKNOWLEDGEMENT

The authors gratefully acknowledge assistance by Dr. Ron Spores at AFRL and by Dr. Ron Cohen at The Aerospace Corporation. Pratt & Whitney wishes to thank both AFRL and The Aerospace Corporation for use of their test facilities and support in carrying out the tests.

### REFERENCES

- <sup>1</sup> E.J. Britt, and J.B. McVey, "Electric Propulsion Activities In U.S. Industries," AIAA-2002-3559, 38<sup>th</sup> AIAA/ ASME/SAE/ASEE Joint Propulsion Conference, Indianapolis, IN, 7-10 July, 2002.
- <sup>2</sup> L.S. Mason, R.S. Jankovsky, and D.H. Manzella, "1000 Hours of Testing on a 10 Kilowatt Hall Effect Thruster," AIAA-2001-3773, 37<sup>th</sup> AIAA/ ASME/SAE/ASEE Joint Propulsion Conference, Salt Lake City, UT, 8-11 July 2001.
- <sup>3</sup> Pratt & Whitney Space Propulsion, San Jose, CA, Unpublished results, April, 2001.
- <sup>4</sup> F. Wilson, D. King, M. Willey, R. Aadland, D. Tilley, and K. de Grys, "Development Status of the BPT Family of Hall Thruster Systems," AIAA 99-2573, 35th AIAA/ASME/SAE/ASEE Joint Propulsion Conference, Los Angeles, CA, 20-24 June, 1999.
- <sup>5</sup> J.M. Fife, et al, "Spacecraft Interaction Test Results of the High Performance Hall System SPT-140," AIAA-2000-3521, 36<sup>th</sup> AIAA/ ASME/SAE/ASEE Joint Propulsion Conference, Huntsville, AL, 16-19 July 2000.
- <sup>6</sup> D.H. Manzella and J.M. Sankovic, "Hall Thruster Ion Beam Characterization," AIAA-95-2927, 31<sup>st</sup> AIAA/ ASME/SAE/ASEE Joint Propulsion Conference, San Diego, CA, 10-12 July 1995.
- <sup>7</sup> E.J. Beiting, "Design and Performance of a Facility to Measure Electromagnetic Emissions from Electric Satellite Thrusters," AIAA-2001-3344, 37<sup>th</sup> AIAA/ ASME/SAE/ASEE Joint Propulsion Conference, Salt Lake City, UT, 8-11 July 2001.
- <sup>8</sup> C. R. Paul, *Introduction to Electromagnetic Compatibility*, John Wiley & Sons, New York, 1992.
- <sup>9</sup> J.E. Pollard and K.D. Diamant, "Hall thruster plume shield wake structure," AIAA-2003-5018, 39<sup>th</sup> Joint Propulsion Conference, Huntsville, AL, 20-23 July 2003.

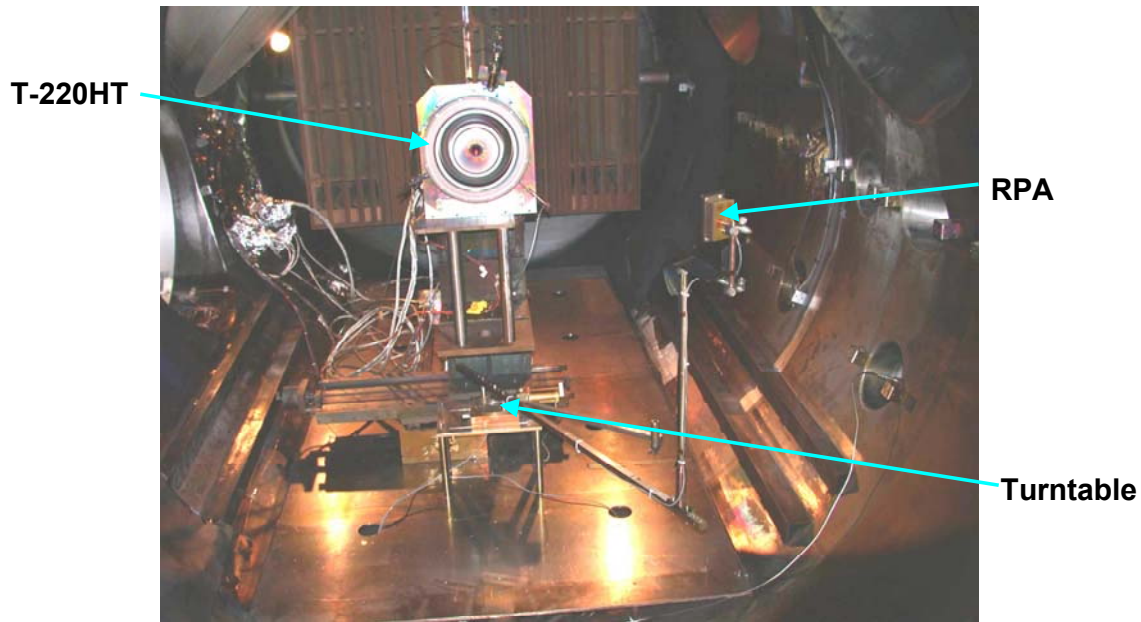


Figure 15. Photograph of T-220HT mounted in position for RPA measurements.

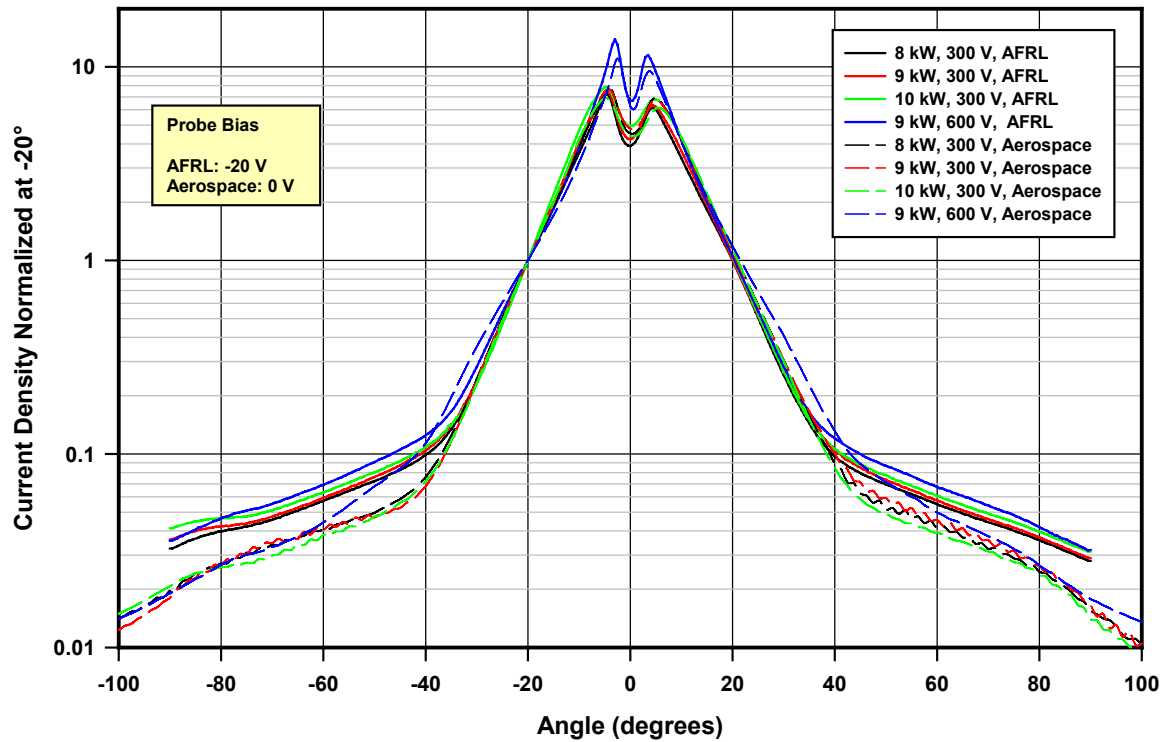


Figure 16. Comparison between plume profiles measured at The Aerospace Corp. and at AFRL. Current densities are normalized at  $-20^\circ$

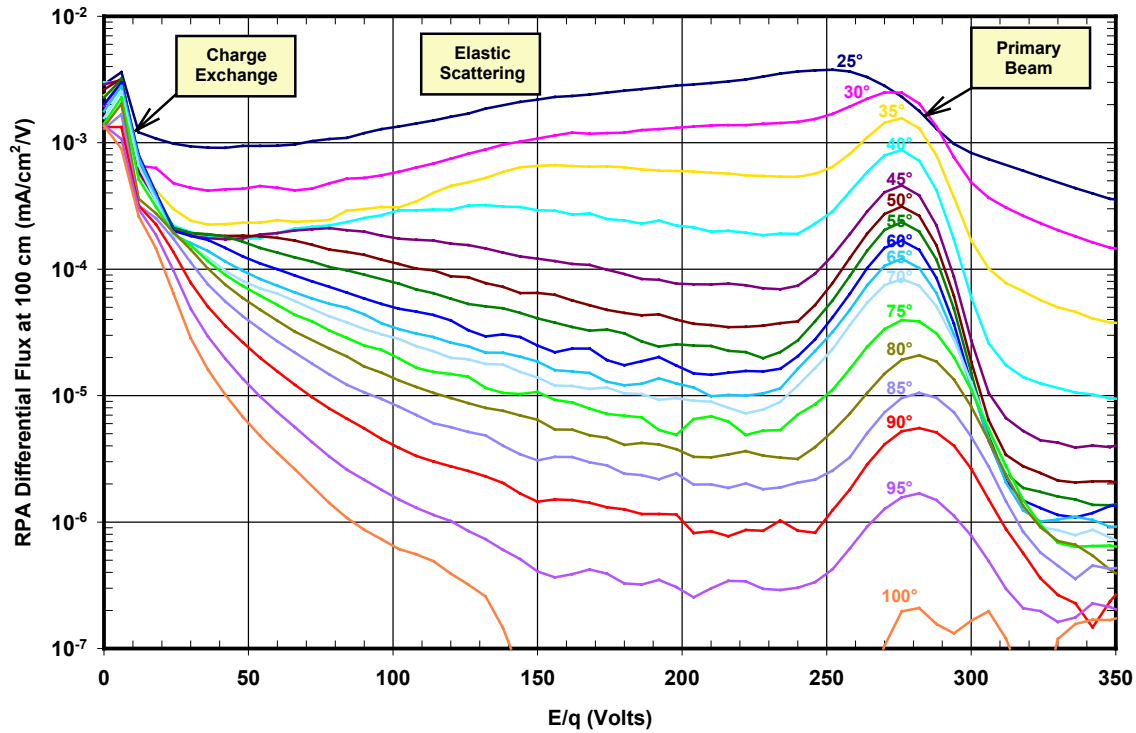


Figure 17. Energy spectra at 9 kW, 300 volts, with angle to beam centerline varying from 25°-100°.

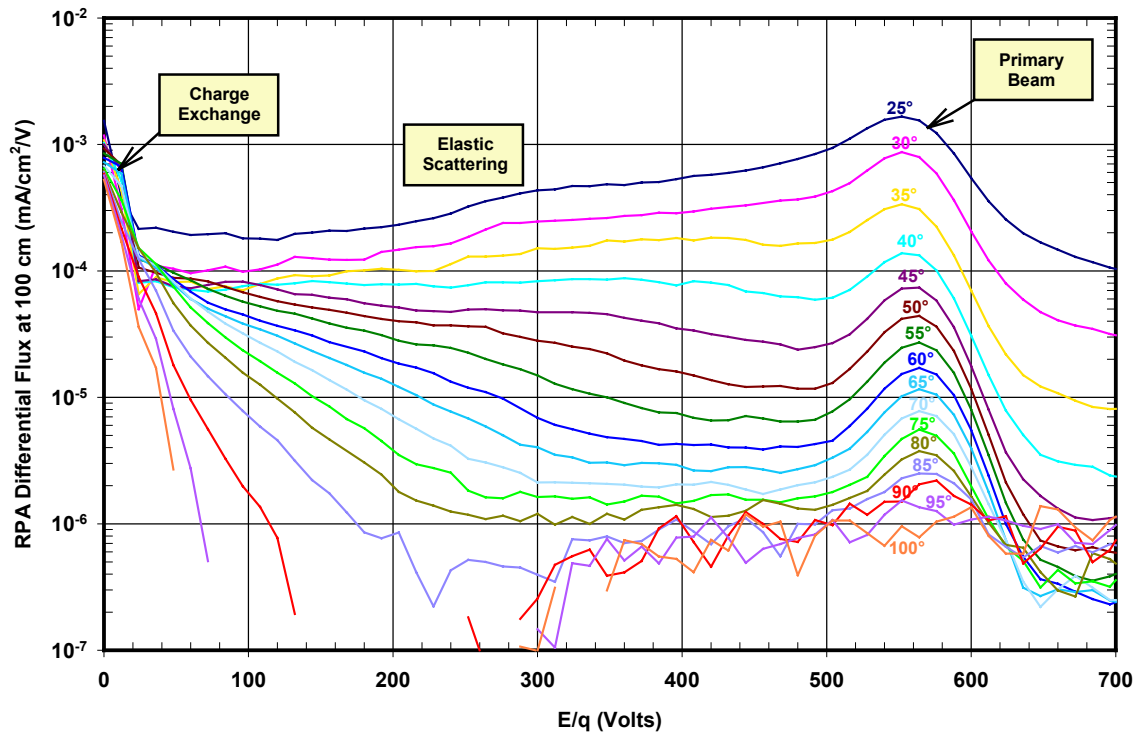


Figure 18. Energy spectra at 9 kW, 600 volts, with angle to beam centerline varying from 25°-100°.

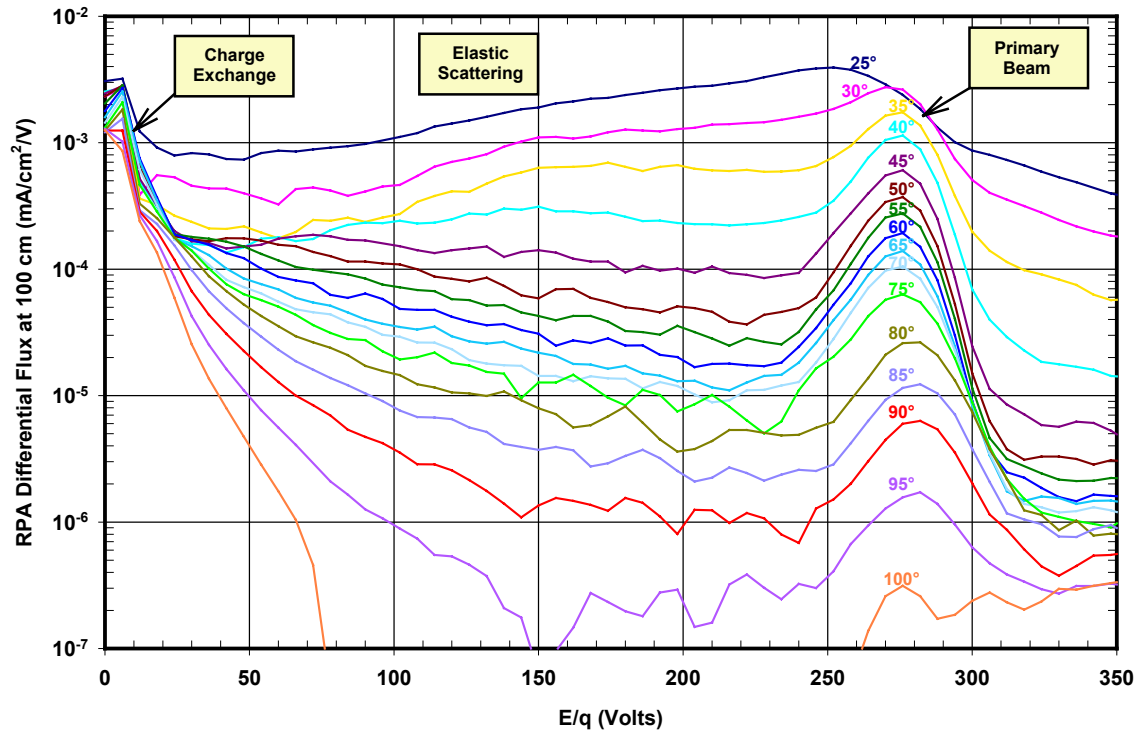


Figure 19. Energy spectra at 8 kW, 300 volts, with angle to beam centerline varying from 25°-100°.

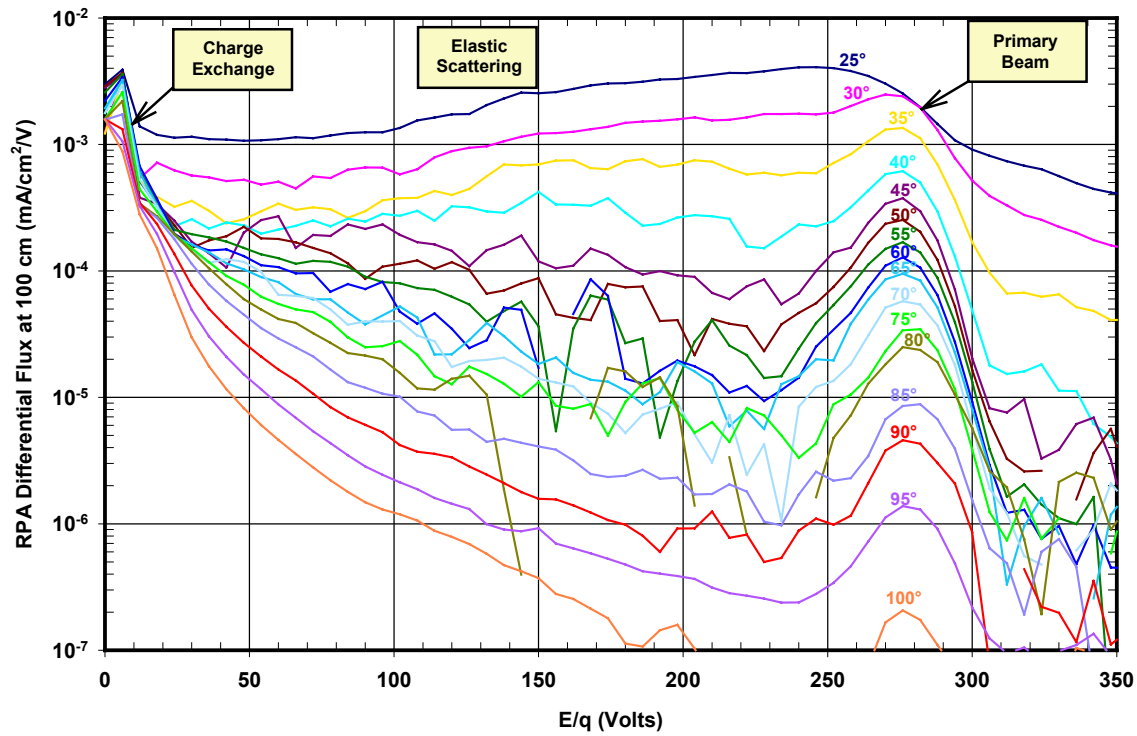


Figure 20. Energy spectra at 10 kW, 300 volts, with angle to beam centerline varying from 25°-100°.